



Optics Letters

Sub-bandgap photo-response of non-doped black-silicon fabricated by nanosecond laser irradiation

CHUN-HAO LI,¹ JI-HONG ZHAO,^{1,3} QI-DAI CHEN,¹ JING FENG,¹ AND HONG-BO SUN^{1,2,4}

¹State Key Laboratory of Integrated Optoelectronics, College of Electronic Science and Engineering, Jilin University, Changchun 130012, China

²State Key Laboratory of Precision Measurement Technology and Instruments, Department of Precision Instrument, Tsinghua University, Haidian, Beijing 100084, China

³e-mail: zhaojihong@jlu.edu.cn

⁴e-mail: hbsun@tsinghua.edu.cn

Received 31 January 2018; revised 1 March 2018; accepted 4 March 2018; posted 5 March 2018 (Doc. ID 321095); published 6 April 2018

Non-doped black silicon (b-Si) is fabricated on the surface layer of a near-intrinsic Si substrate by nanosecond (ns) laser direct writing in an argon (Ar) atmosphere. The non-doped samples exhibit a near-unity sub-bandgap (1100 ~ 2500 nm) absorptance of more than 50%. Amazingly, the resistivity of the ns laser irradiated b-Si layer is about five orders of magnitude lower than that of the unprocessed Si substrate. The carrier density of the b-Si layer is about $1 \times 10^{18} \text{ cm}^{-3}$, according to the Hall effect measurement. Temperature-dependent Hall effect measurements show that the non-doped b-Si layer exhibits an energy level of 0.026 eV below the conduction band minimum (CBM). At last, Si infrared photodiodes are made based on the difference of carrier concentration between the ns laser-processed b-Si layer and the high-resistivity Si substrate. The responsivity of the b-Si photodiode for 1310 nm is up to 256 mA/W at a 10-V reverse bias, which is much higher than that of the reported pure Si bulk-structure photodiodes. © 2018 Optical Society of America

OCIS codes: (140.3390) Laser materials processing; (220.4000) Microstructure fabrication; (040.5160) Photodetectors; (040.3060) Infrared.

<https://doi.org/10.1364/OL.43.001710>

In the past thirty years, silicon (Si) photonics, as a novel technique for large-scale optical-electronic integration, have been used for optical communication and optical interconnection [1]. Si photonics technology can not only extend the transmission rate and the transmission bandwidth of modern communication techniques, but such technology can also satisfy the low-coast complementary metal-oxide-semiconductor transistor (CMOS) compatibility criteria [2]. So far, among all of the Si photonics components, low-loss Si waveguides, high-speed Si optical modulators, and optical pumping lasers have already been obtained in the last years; but the development of high-performance Si photo-detectors at optical communication

wavebands has remained as unaccomplished task [3]. The Si crystal is transparent to infrared light at communication wavebands, due to its 1.12-eV bandgap. To realize silicon-based infrared light detection, narrow-gap semiconductors (Ge, InGaAs, PbS, etc.) are usually compounded to the Si platform through either epitaxial growth or bonding technology. However, these technologies will increase the processing complexities and compromise the CMOS compatibility [2].

An effective method to extend the absorption waveband of Si is the hyper-doping technique. In the hyper-doped Si samples, supersaturated impurities (such as S, Se, Te, N, and P) can be doped into the Si surface layer via pulsed laser irradiation or ion implantation [4–7]. The supersaturated impurities can introduce energy levels and even intermediate bands in the Si bandgap, which can contribute to a broad sub-bandgap absorption [4,8]. Photodiodes based on these materials exhibit very high photo-response around the band-edge region [9–11]. For example, photodiode with a responsivity of 100 A/W for 1064 nm has been obtained by Carey *et al.* in S-hyper-doped Si materials [10]. However, the responsivity of the above S-doped photodiode decreases dramatically with the increase of the optical wavelength and the responsivity is merely 50 mA/W for 1310-nm light [10]. The main reason is that, in the supersaturated S-doped Si materials there is an ultra-high background free carrier concentration induced by the hyper-doped impurities, which hinders the performance of infrared photo-detectors.

In this study, we demonstrate non-doped Si infrared photodiodes with a photo-responsivity of 256 mA/W for 1310 nm, which is based on the junction between the nanosecond (ns) laser-treated Si surface layer and the near-intrinsic Si substrate. The novel optical and electronic properties of non-doped b-Si make it a very promising material for making pure Si infrared photo-detectors.

The experiment is carried out with a frequency-tripled, Q-Switched, Nd:YAG ns laser (spectral physics, a 10-ns pulse duration, a 355-nm wavelength, and a 10-Hz repetition rate). After the laser emitted, an expansion system and a diagram are used for achieving a uniformly distributed laser beam with a

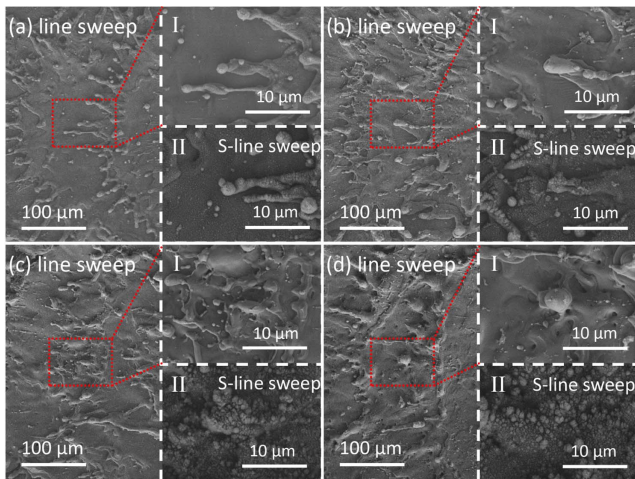


Fig. 1. Top-view SEM images of the non-doped b-Si samples irradiated via single-line scanning with laser fluencies of (a) 19.7 J/cm^2 , (b) 39.4 J/cm^2 , (c) 78.8 J/cm^2 , and (d) 118.2 J/cm^2 ; inserts (I) are the magnified images corresponding to the selected region in the red dash squares; inserts (II) show the morphologies of the non-doped b-Si fabricated by S-line scanning.

8-mm diameter, which is then focused by a 600-mm lens and incidents directly to the Si substrate (n-type, $\langle 111 \rangle$, $4000 \Omega \cdot \text{cm}$, $250 \mu\text{m}$ thick). The diameter of the focused laser spot on the Si surface is about $180 \mu\text{m}$, which is measured by CCD. The Si substrate, with a surface area of $15 \text{ mm} \times 15 \text{ mm}$, is equipped on a 2D translation stage, and the Si surface is totally processed via continuously moving the translation stage in a S-line-scan route. The scanning speed is $250 \mu\text{m/s}$, and the space between two adjacent lines is $100 \mu\text{m}$. During the laser irradiation process, the Si substrate is mounted on a vacuum chamber, which is filled with 0.1-MPa argon (Ar) gas.

After the ns laser irradiation, the morphology of the b-Si samples is measured with a field emission-scanning electron microscope (SEM, JEOL JSM-7500F, and Japan). The absorption spectrum of the b-Si samples is characterized by a spectrophotometer (UV-3600, Company) equipped with an integrating sphere (LISR-UV3100). To analyze the electrical properties of the non-doped b-Si samples, a RST-5 four-point probes resistivity measurement system and an ACCENT HL5500PC Hall system based on the Van der Pauw method are used. A Keithley 2400 sourcemeter is used for obtaining the I-V properties of the non-doped b-Si infrared photodiodes.

Figure 1 shows the top-view SEM images of the b-Si surface morphologies processed with single-line scanning. The laser fluencies used here are (a) 19.7 J/cm^2 , (b) 39.4 J/cm^2 , (c) 78.8 J/cm^2 , and (d) 118.2 J/cm^2 , respectively. In Figs. 1(a)–1(d), overlapped thermal-melting zones are observed. Diameters of the melting zones increase with increased laser fluencies. Radiated branches are formed at the edge of the melting zones, as shown in the insets (II). During this line-by-line scanning process, the Si surface is covered with nano-particles sputtered from the adjacent line. Increasing the laser fluencies will enlarge the diameters of the sputtered particles and the surface roughness. The depth of modified layer varies from several hundred nanometers to several micrometers for the selected laser fluencies. The rough surface layer can act as an antireflective coating.

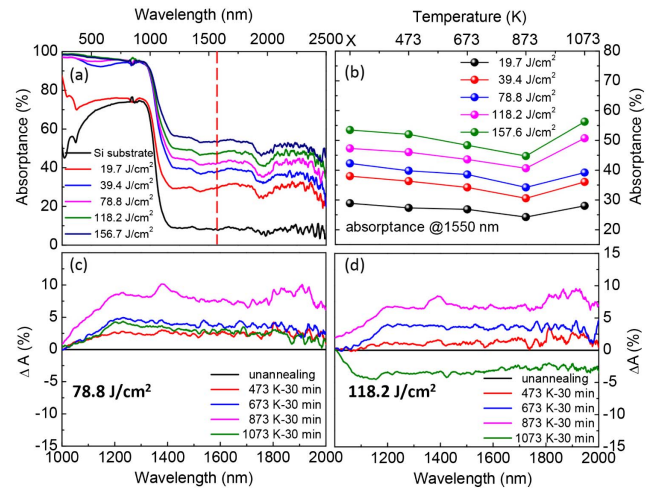


Fig. 2. (a) Absorbance of b-Si samples fabricated by ns laser irradiation in Ar with different laser fluencies; (b) temperature-dependent absorbance at 1550 nm , the annealing time for all the samples are 30 min and label X in horizontal ordinate means the sample is not annealed; (c) and (d) are the sub-bandgap absorbance variation of the b-Si samples irradiated with 78.7 J/cm^2 and 118.2 J/cm^2 .

Figure 2(a) shows the absorption spectra of the unprocessed Si substrate and the b-Si samples irradiated with different laser fluencies of (a) 19.7 J/cm^2 , (b) 39.4 J/cm^2 , (c) 78.8 J/cm^2 , (d) 118.2 J/cm^2 , and (e) 157.6 J/cm^2 , respectively. The above-bandgap absorbance of b-Si samples is more than 90%. The corresponding reflectance is less than 10%, which is comparable plasma etching and ICP etching [12,13]. It means that the rough Si surface layer exhibits excellent light-trapping abilities [14]. The sub-bandgap absorbance of b-Si samples are approximately constant at the wavelengths of $1100\text{--}2500 \text{ nm}$ and increase gradually from 30% to 60% with the increase of laser fluence. The sub-bandgap absorption is related to the defect states (Urbach states or deep-level structural defects in the re-solidified surface layer) in the b-Si layer and can be further enhanced by the textured Si surface [7,15]. Figure 2(b) shows the absorbance of b-Si samples at the wavelength of 1550 nm after annealed at different temperatures (label X in horizontal ordinate means the samples are not annealed). The annealing time for all the samples is 30 min. The samples' absorbance at 1550 nm gradually decreases with thermal annealing temperatures up to 873 K . The small reduction of absorbance for the annealed samples is due to the decrement of the unstable Urbach states after thermal treatment. However, an enhancement of sub-bandgap absorbance is observed for samples annealed above 1073 K . This phenomenon, which is called absorption reactivation, was reported in the sulfur hyper-doped b-Si, and it was attributed to the point defects stabilized at high temperature [16]. Figures 2(c) and 2(d) present the absorption variations (ΔA) of b-Si samples at the wavelengths from $1 \mu\text{m}$ to $2 \mu\text{m}$. The samples are irradiated with laser fluencies of 78.8 J/cm^2 [Fig. 2(c)] and 118.2 J/cm^2 [Fig. 2(d)], respectively. Here, ΔA is defined as $\Delta A = A_b - A_a$, where A_b and A_a represent the absorbance before and after annealing, respectively. The ΔA values of the samples annealed at 1073 K [green lines in Figs. 2(c) and 2(d)] are lower than that of the 873 K annealed samples [pink lines in Figs. 2(c) and 2(d)]; it means

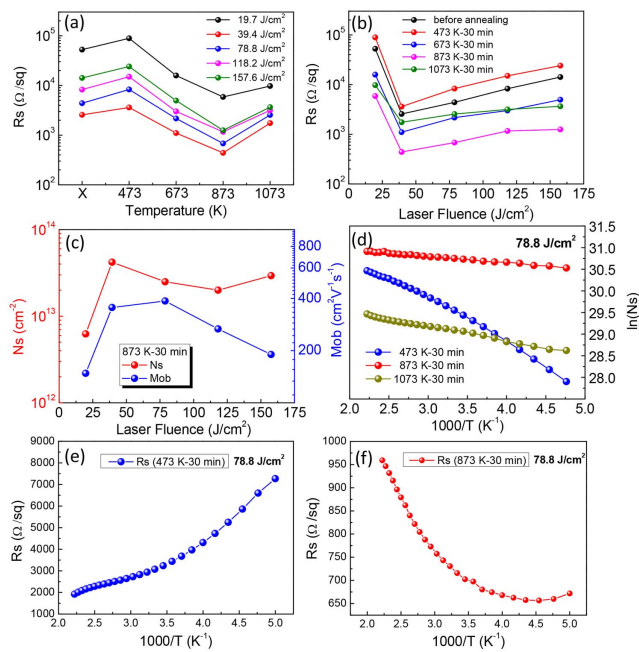


Fig. 3. (a) and (b) exhibit the resistance of the non-doped b-Si samples fabricated with different laser fluencies and annealing temperatures. X means the samples are not annealed; (c) Hall effect measurements for sheet carrier concentration and carrier mobility of the b-Si samples fabricated at different laser fluencies. All the samples are annealed at 873 K for 30 min. (d) Temperature-dependent Hall effect measurement results of b-Si samples annealed at different temperatures; (e) and (f) are temperature-dependent resistance of the b-Si samples annealed at 473 K and 873 K, respectively.

that the absorption in these wavebands is reactivated after a high-temperature thermal annealing process. As shown in Fig. 2(d), the reactivated absorbance is larger than that of the unannealed sample, so the calculated ΔA value is negative (green line). The high sub-bandgap absorption guarantees non-doped b-Si a promising material for infrared-light detection.

To further evaluate the light-detection ability of the non-doped b-Si, the electrical properties of the b-Si samples are examined. Figures 3(a) and 3(b) show that the square resistance (R_{\square}) of the b-Si samples depends on annealing temperatures (label X in horizontal ordinate means the samples are not annealed) and laser fluencies. The R_{\square} values of the b-Si samples are in the range of 4×10^2 – $5 \times 10^5 \Omega/\square$. The resistivity (ρ) values of the b-Si samples can be calculated according to $\rho = R_{\square} * l$, where l is the thickness of the re-solidified layer, and it is estimated to be $0.5 \sim 1 \mu\text{m}$ [15,17]. The calculated resistivity of the non-doped b-Si is $0.02 \sim 50 \Omega \cdot \text{cm}$, which is about 5 orders of magnitude lower than that of the unprocessed Si substrate ($4000 \Omega \cdot \text{cm}$). We should note that the non-doped samples are fabricated in an ambient of argon, which is an inert gas and cannot gain or loss electrons in Si system, so it cannot provide any free carriers to the b-Si layer. It means the reduction of resistivity is induced by other mechanisms except doping. The variation tendency of resistivity as thermal annealing temperature and laser fluence is the result of the combination of multi-defects in the b-Si layer. Defects in the non-doped b-Si layer are very complicated; there are dangling bonds and trap states in the amorphous Si or the polycrystalline Si,

as well as the ns laser-induced defects (such as di-vacancy V-V, multi-vacancy center, vacancy-oxygen complex, clusters of vacancy, and vacancy-impurity associations) [16]. At a proper annealing temperature and a proper laser fluence, the electrical activity of defect states can be activated. And a minimum resistance of $400 \Omega/\square$ is achieved with $39.4 \text{ J}/\text{cm}^2$ laser fluence and an 873-K annealing temperature. Further increasing or decreasing the laser fluence or the annealing temperature can enhance the Si resistance.

Figure 3(c) presents the Hall effect measurement results of the sheet carrier density (N_s , absolute value) and the carrier mobility (Mob) of the b-Si samples. The obtained N_s values are negative, meaning that the conduction type of the b-Si layer is n-type. The sheet carrier density is in the range of 6×10^{12} – $5 \times 10^{13} \text{ cm}^{-2}$, corresponding to a body carrier density of 6×10^{16} – $1 \times 10^{18} \text{ cm}^{-3}$, which is much larger than the that of the Si substrate ($\sim 4 \times 10^{11} \text{ cm}^{-3}$). Thus, the defect density with electrical activity also can be estimated to be 10^{18} cm^{-3} [18]. The concentration gradient between the Si substrate and the b-Si layer can induce a N^+ -N certification junction, which is the foundation of building the b-Si photodiode. The non-doped b-Si exhibits a high mobility of $400 \text{ cm}^2 \text{ V}^{-1} \text{ s}^{-1}$, which is about 2–4 times larger than that of the hyper-doped Si samples [7]. It means the non-doped material is more suitable in light-detection applications than the hyper-doped b-Si. Temperature-dependent Hall effect measurements of the non-doped b-Si fabricated at $78.8 \text{ J}/\text{cm}^2$ are shown in Fig. 3(d). The energy level (E_i) of the defect states of the b-Si layer is calculated according to $\ln(N_s) \propto -(E_i)/(2k)/T$, where N_s is the sheet carrier density, k is the Boltzmann constant, and T is the temperature [19]. When annealed at 473 K, the Si exhibits an energy level (intermediate level) of 0.173 eV below the conduction band minimum (CBM). When the annealing temperature increases to 873 K, the energy level decreases to 0.026 eV, meaning that the concentration of the electrical activated defect states increase dramatically. This shallow donor level can provide a certain amount of free carriers to the b-Si layer, and then induce a reduction of the resistance, which is in consistent with the R_{\square} values obtained by four-point probes resistivity measurement shown in Fig. 3(a). A higher temperature annealing of 1073 K can increase the energy of the intermediate level to 0.032 eV due to the elimination of the electrical activated defects. We should note that the calculated intermediate levels are too shallow and narrow to contribute to the broadband light absorption [see Fig. 2(a)], so the E_i values should be equivalence results of all the intermediate levels or bands induced by laser irradiation. Figures 3(e) and 3(f) are the temperature-dependent R_{\square} values of the b-Si samples fabricated with $78.8 \text{ J}/\text{cm}^2$ laser fluence and annealed at 473 K and 873 K, respectively. In Fig. 3(e), the R_{\square} values decrease with the increasing of the temperature, since a higher temperature will increase the carrier concentration or decrease the Si resistance. However, for the b-Si annealed at 873 K [Fig. 3(f)]. The R_{\square} values slowly raise below 220 K and then rapidly increase with the increasing temperature in the range of 220–500 K, which shows metallization-like properties.

At last, pure Si infrared photodiodes are fabricated with the non-doped b-Si material. The schematic diagram of photodiodes is shown in Fig. 4. The non-doped b-Si materials are fabricated with a $78.8 \text{ J}/\text{cm}^2$ laser fluence and cut into $5 \text{ mm} \times 5 \text{ mm}$ squares. After that, the b-Si samples are annealed at

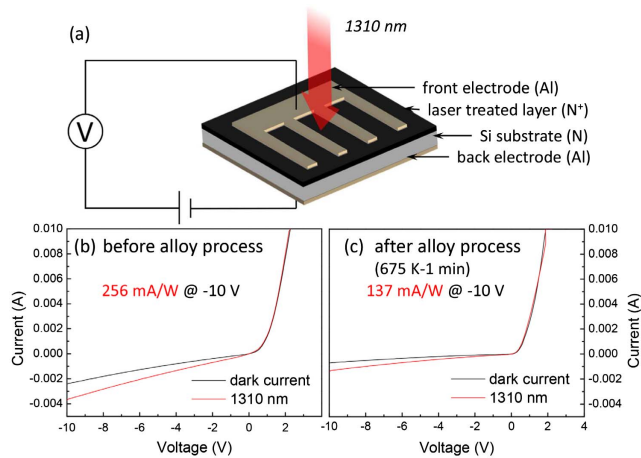


Fig. 4. (a) Schematic diagram of the non-doped b-Si photodiode. (b) The photo current and dark current versus voltage characteristics for the b-Si photodiode before and after alloy annealing (1 min at 675 K for) respectively.

873 K for 30 min and dipped into a diluted HF solution (5%) to remove the native oxide surface layer. Afterwards, fingerlike aluminum (Al) electrode is thermally evaporated onto the b-Si surface layer as a front electrode. Then, the Si back surface is coated with Al film (back electrode) to form an Ohmic contact. As shown in Fig. 4(b), the non-doped b-Si photodiode exhibits obvious rectification characteristics because of the N^+-N rectification junction between the b-Si layer and the crystalline Si substrate. At a reverse bias of 10 V, the photodiode shows a responsivity of 256 mA/W for 1310-nm infrared light. Inevitably, this b-Si photodiode exhibits a relatively high dark current density of 9.76 mA/cm² at -10 V, which may be related to the laser-induced defects in the surface layer. To reduce the interfacial defect density and increase the minority carrier lifetime in the b-Si layer, a 200-nm Al₂O₃ passivation layer is deposited on the b-Si surface via atomic layer deposition (ALD). Disappointedly, surface passivation shows unremarkable effects on reducing the dark current density of the non-doped photodiode. However, we find that alloy annealing turns out to be an effective method to improve the performance of the non-doped b-Si photodiode. After annealed at 748 K for 1 min, the photodiode's dark current reduces to 2.88 mA/cm² [as shown in Fig. 4(c)], which is about 3.4 times lower than that of the unannealed photodiode. The responsivity of the annealed photodiode at 1310 nm reduces to 137 mA/W, but it is still much larger than the reported bulk-structure Si-based photodiodes. The non-doped b-Si material exhibits great potentiality in making Si-based infrared photodiode.

In conclusion, the non-doped b-Si samples are fabricated by ns-laser direct writing in an argon atmosphere. The laser-irradiated b-Si samples exhibit high absorption in both the visible wavelengths and the infrared region due to the textured surface layer and the pulsed laser-induced defect states. A donor level of 0.026 eV, which is related to the laser induced defects, is observed in the b-Si layer. By adjusting the laser fluence and annealing temperature, we achieved b-Si samples with a

minimum resistivity of 0.02 $\Omega \cdot \text{cm}$, which is 5 orders of magnitude larger than that of the Si substrate. A N^+-N rectification junction is formed between the b-Si layer and the crystalline Si substrate. An infrared photodiode worked at infrared waveband is made based on the non-doped b-Si material. At a reverse bias of 10 V, the infrared photodiode exhibits a record responsivity of 256 mA/W for 1310 nm light. Alloy annealing at 748 K for 1 min can decrease the devices' responsivity to 137 mA/W, however, the signal-to-noise ratio of the photodiode can be improved at the same time.

Funding. National Key Research and Development Program of China (2017YFB1104300); National Natural Science Foundation of China (NSFC) (#61775077, #61590930, #61435005, #51335008).

REFERENCES

- H. Chen, V. Corbaliou, A. S. Solntsev, D. Choi, M. A. Vincenti, D. D. Ceglia, C. D. Angelis, Y. Lu, and D. N. Neshev, *Light Sci. Appl.* **6**, e17060 (2017).
- J. P. Malloa, A. J. Akey, C. B. Simmons, D. Hutchinson, J. Mathews, J. T. Sullivan, D. Recht, M. T. Winkler, J. S. Williams, J. M. Warrender, P. D. Persans, M. J. Aziz, and T. Buonassisi, *Nat. Commun.* **5**, 3011 (2014).
- A. Annoni, E. Guglielmi, M. Carminati, G. Ferrari, M. Sampietro, D. A. B. Miller, A. Melloni, and F. Morichetti, *Light Sci. Appl.* **6**, e17110 (2017).
- C. Wu, C. H. Crouch, L. Zhao, J. E. Carey, R. Younkin, J. A. Levinson, and E. Mazur, *Appl. Phys. Lett.* **78**, 1850 (2001).
- M. A. Sheehy, B. R. Tull, C. M. Friend, and E. Mazur, *Mater. Sci. Eng. B* **137**, 289 (2007).
- X. Dong, N. Li, Z. Zhu, H. Shao, X. Rong, C. Liang, H. Sun, G. Feng, L. Zhao, and J. Zhuang, *Appl. Phys. Lett.* **104**, 091907 (2014).
- C. H. Li, J. H. Zhao, X. Y. Yu, Q. D. Chen, J. Feng, and H. B. Sun, *IEEE Photon. J.* **8**, 6805809 (2016).
- Z. Zhu, H. Shao, X. Dong, N. Li, B. Y. Ning, X. J. Ning, L. Zhao, and J. Zhuang, *Sci. Rep.* **5**, 10513 (2015).
- L. Y. Du, Z. M. Wu, R. Li, F. Tang, and Y. D. Jiang, *Opt. Lett.* **41**, 5031 (2016).
- J. E. Carey, C. H. Crouch, M. Shen, and E. Mazur, *Opt. Lett.* **30**, 1773 (2005).
- X. Y. Wang, Y. G. Huang, D. W. Liu, X. N. Zhu, and H. L. Zhu, *Chin. Phys. Lett.* **30**, 036101 (2013).
- A. Balčytis, M. Ryu, G. Seniutinas, Y. Nishijima, Y. Hikima, M. Zamengo, R. Petruškevičius, J. Morikawa, and S. Juodkazis, *Opt. Eng.* **54**, 127103 (2015).
- Y. Nishijima, R. Komatsu, S. Ota, G. Seniutinas, A. Balčytis, and S. Juodkazis, *APL Photon.* **1**, 076104 (2016).
- P. Ščajev, T. Malinauskas, G. Seniutinas, M. D. Arnold, A. Gentle, I. Aharonovich, G. Gervinskas, P. Michaux, J. S. Hartley, E. L. H. Mayes, P. R. Stoddart, and S. Juodkazis, *Sol. Energ. Mat. Sol. C* **144**, 221 (2016).
- C. H. Li, J. H. Zhao, Q. D. Chen, J. Feng, W. T. Zheng, and H. B. Sun, *IEEE Photon. Technol. Lett.* **27**, 1481 (2015).
- B. K. Newman, M. J. Sher, E. Mazur, and T. Buonassisi, *Appl. Phys. Lett.* **98**, 251905 (2011).
- M. J. Smith, Y. T. Lin, M. J. Sher, M. T. Winkler, E. Mazur, and S. Gradečak, *J. Appl. Phys.* **110**, 053524 (2011).
- X. W. Wang, R. Buividas, F. Funabiki, P. R. Stoddart, H. Hosono, and S. Juodkazis, *Appl. Phys. A* **122**, 194 (2016).
- X. Y. Yu, J. H. Zhao, C. H. Li, Q. D. Chen, and H. B. Sun, *IEEE Trans. Nanotechnol.* **16**, 502 (2017).